BIOCHEMISTRY
including biophysical chemistry & molecular biology

Article

pubs.acs.org/biochemistry

Catalytic Mechanism of Bacteriophage T4 Rad50 ATP Hydrolysis

Timothy J. Herdendorf and Scott W. Nelson*

Department of Biochemistry, Biophysics, and Molecular Biology, Iowa State University, Ames, Iowa 50011, United States

Supporting Information

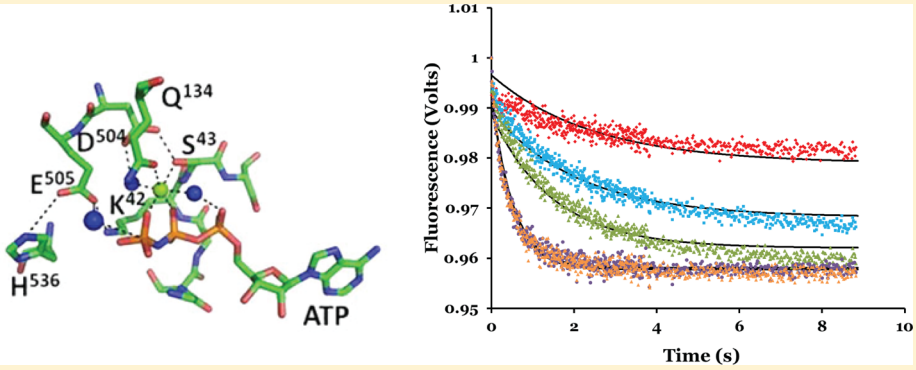

ABSTRACT: Spontaneous double-strand breaks (DSBs) are one of the most deleterious forms of DNA damage, and their improper repair can lead to cellular dysfunction. The Mre11 and Rad50 proteins, a nuclease and an ATPase, respectively, form a well-conserved complex that is involved in the initial processing of DSBs. Here we examine the kinetic and catalytic mechanism of ATP hydrolysis by T4 Rad50 (gp46) in the presence and absence of Mre11 (gp47) and DNA. Single-turnover and pre-steady state kinetics on the wild-type protein indicate that the rate-limiting step for Rad50, the MR complex, and the MR-DNA complex is either chemistry or a conformational change prior to catalysis. Pre-steady state product release kinetics, coupled with viscosity steady state kinetics, also supports that the binding of DNA to the MR complex does not alter the rate-limiting step. The lack of a positive deuterium solvent isotope effect for the wild type and several active site mutants, combined with pH−rate profiles, implies that chemistry is rate-limiting and the ATPase mechanism proceeds via an asymmetric, dissociative-like transition state. Mutation of the Walker A/B and H-loop residues also affects the allosteric communication between Rad50 active sites, suggesting possible routes for cooperativity between the ATP active sites.

DNA double-strand breaks (DSBs) are one of the most harmful types of DNA damage.[1] In humans, DSBs occur, on average, 50 times per cell cycle[2] and arise during normal physiological processes. Examples of these processes include free radical production, class-switch recombination for antibody effector modulation,[3,4] Spo11-dependent DSB during meiosis,[5] and the collapse of a stalled replication fork during DNA replication.[6,7] DSBs are also the product of exposure to ionizing radiation and various genotoxic chemicals (i.e., camptothecin and methyl-methanesulfonate). In *Saccharomyces cerevisiae*, resection of the DSB follows a two-step pathway in which the MR complex plays an essential role in the first step by working with Xrs2 and Sae2 to remove 20−100 nucleotides from the 5′ end of the DSB.[8] In the second step, the recessed 5′ end is further degraded by either Sgs1/Top3/RmiI protein with RPA or ExoI with RPA. Following resection, Rad51 catalyzes invasion of the ssDNA into a region of homologous DNA, creating a D-loop that is used as a primer for DNA synthesis. After completion of DNA synthesis, either the extended strand is liberated from the template by a DNA helicase or the Holliday junction is resolved by a DNA nuclease and ligase.

In bacteriophage T4, the MR complex is absolutely essential and is required for recombination-dependent replication (RDR) and DSB repair.[9] The nuclease activity of Mre11 is critically important for phage growth and RDR, as nuclease-deficient active site mutants of T4Mre11 display slow phage growth and completely eliminate RDR. In addition to its probable role in DNA end processing, it has been shown that the MR complex plays an important role in the coordinated repair of the two ends of a DSB.[9]

Rad50 is a member of the ATP binding cassette (ABC) protein superfamily. The ABC protein superfamily is one of the largest and most highly conserved families known, and its members are found in large numbers in all organisms.[10] The common feature of ABC proteins is the nucleotide binding domain (NBD), which is dimeric and binds and/or hydrolyzes ATP at its dimeric interface.[11] These proteins couple ATP hydrolysis to mechanical motion (i.e., metabolite transport and DNA translocation) and are generally considered to be allosteric enzymes. ABC ATPases contain six conserved motifs. These motifs are the Walker A- and B-motifs,[12] the Q-loop (glutamine loop), the C-motif (or signature motif), the H-loop,

Received: May 9, 2014
Revised: August 15, 2014
Published: August 19, 2014

   dx.doi.org/10.1021/bi500558d | *Biochemistry* 2014, 53, 5647−5660

and the D-loop. These motifs contribute residues that compose the ATP active site. On the basis of several crystal structures,[13−16] the Walker A/B-, Q-, and H-motifs from one monomer and the C-motif and D-loop from the second monomer act in trans to complete the active site. The Walker A serine (S43), Q134 (Q-loop), and Walker B aspartate (D504) are shown to coordinate, either directly or indirectly through a mediating water, to the magnesium of the MgATP complex (the residue numbering corresponds to the T4 bacteriophage Rad50). Two residues located in the C-motif have recently been implicated in the binding of the MgATP complex.[17] The mutant proteins S471A and E474Q have inflated $S_{0.5}$ and K_d values (10- and 25-fold higher $S_{0.5}$ values, respectively, and 11- and 21-fold higher K_d values, respectively), with little perturbation in k_{cat} (≤5-fold).

Bacteriophage T4 Rad50 is a relatively slow ATPase, but ATP turnover is accelerated ∼20-fold in the presence of Mre11 and DNA (MR-D).[18] The mechanism of this allosteric activation remains unknown. Considering this activation occurs only in the presence of both Mre11 and DNA, a pathway must exist between the binding sites of Mre11 and DNA and the active site of Rad50.[19] This conformational change must rearrange the ATP active site leading to an accelerated catalytic cycle. The kinetic step in the cycle that is accelerated is unclear, as the rate-limiting step is unknown. To fully understand the mechanism of ATPase activation by Mre11 and DNA, the rate-limiting step of the reaction must be determined for Rad50 alone and for the MR-D complex. In addition to Rad50 being activated by Mre11 and DNA, its ATPase activity becomes more positively cooperative for the MR-D complex compared to that of Rad50 alone (Hill coefficients of 2.4 and 1.4, respectively).[18] It stands to reason that mutation of certain active site residues should disrupt this communication and lead to a starting point of the pathway of communication between the two active sites.

To probe the mechanism of ATPase activity, several active site residues were mutated (S43, D504, E505, and H536) and kinetically evaluated. The data reported here suggest that chemistry is rate-limiting for Rad50, the MR complex, and the MR-D complex ATPase reaction. Additionally, indirect evidence, which includes pre-steady state kinetics of product release, steady state viscosity specific activity determination, and mutational analysis, also suggests that chemistry is rate-limiting in the MR-D complex. The absence of a deuterium solvent isotope effect suggests ATP hydrolysis proceeds through a dissociative mechanism.

MATERIALS AND METHODS

Materials. Oligodeoxynucleotides used for mutagenesis were purchased from either Integrated DNA Technologies or the Iowa State University DNA Facility. *Pfu* DNA polymerase Ultra was purchased from Agilent Technologies, Inc. Phusion High-Fidelity DNA Polymerase was purchased from Thermo Scientific. The expression vector used for subcloning of the *Escherichia coli* phoS gene was a pET28 plasmid purchased from Novagen. Plasmid DNA was propagated in *E. coli* XL-1 Blue cells (Agilent Technologies, Inc.). Kits for plasmid DNA purification were purchased from Qiagen. DNA sequencing was performed at the Iowa State University DNA Facility. *E. coli* BL21(λDE3) cells were obtained from Novagen. Isopropyl β-D-thiogalactopyranoside (IPTG) and antibiotics (ampicillin and kanamycin) were purchased from Gold Biotechnology. Chitin beads were purchased from New England Biolabs. Coupling enzymes (pyruvate kinase and lactate dehydrogenase), dNTPs, nicotinamide adenine dinucleotide (NADH), and nickel-agarose were purchased from Sigma-Aldrich Chemical Co. Phosphoenolpyruvate was purchased from Alfa Aesar. Adenosine 5′-triphosphate was purchased from USB Corp. Components of the media were purchased from Boston Bioproducts. Unless otherwise stated, chemicals were purchased from Fisher Scientific. N38A and D512A Rad50 were previously purified.[32]

Mutagenesis, Protein Expression and Purification, and Steady State ATPase Kinetics. Mutagenesis, expression and purification, and the steady state ATPase kinetics were conducted as previously described.[18]

Determination of an Equilibrium Dissociation Constant for ATP by Intrinsic Tryptophan Fluorescence. All fluorescence measurements were performed using a Cary Eclipse spectrofluorometer (Varian). The intrinsic tryptophan fluorescence of S43A (1 μM), D504N (0.53 μM), E505Q (0.67 μM), H536A (0.63 μM), H536Q (0.63 μM), and E505Q/H536A (0.53 μM) was measured at 30 °C in 3.0 mL of 50 mM Tris-HCl, 50 mM KCl, and 5 mM $MgCl_2$ (pH 8.0). Samples were excited at 295 nm, and the emission was monitored at 335 nm. For data analysis, values measured at the fluorescent emission peak of 335 nm were corrected for dilution and any ATP inner filter effect. Thus, these corrected fluorescence data were plotted against ATP concentrations and fit in Dynafit (Biokin, Ltd.[20]) to a standard equilibrium mechanism. The K_d estimates reflect the average of at least three separate titrations.

Evaluation of Nuclease Activity. Estimates of nuclease activity were determined as previously described,[18] with the exception of the 2-aminopurine probe for the 3′ DNA substrate being located at position 1 with respect to the 3′ end instead of position 2. Oligo sequences are reported in the Supporting Information.

Pre-Equilibrium Kinetics of Tryptophan Quenching upon ATP Binding. The pre-equilibrium kinetics for the binding of ATP to Rad50 was monitored using a Bio-Logic stopped-flow apparatus equipped with an SFM 4000 rapid mixer coupled to a MOS 500 spectrophotometer (Bio-Logic Science Instrument SA, Claix, France). Acquisition parameters were as follows: 295 nm excitation, 5 nm bandwidth, 320 nm long pass filter, and 410 V applied to the PMT with sampling every 0.5 ms (8000 points, 4 s) followed sampling every 1 ms (8000 points, 8 s). The rate of quenching was determined at 12 ATP concentrations (17 μM to 15 mM). Assay included 50 mM Tris-HCl (pH 7.6, 30 °C), 50 mM KCl, 25 mM $MgCl_2$, and 3 μM Rad50. The progress curves at each ATP concentration (each an average of at least four individual shots) were globally fit to a rapid equilibrium mechanism followed by a conformational change using Dynafit3 (Biokin, Ltd.[20]). An additional mechanism, which included a chemical step following the conformational change, was also tested. The resulting microscopic rate constant estimates are the average of three complete data sets. These estimates were used to calculate a kinetic dissociation constant using the equation $K_d = (k_2k_4)/(k_1k_3)$.

Preparation of the Fluorescent Sensor of Inorganic Phosphate. Plasmid pSN5182/N containing the mutated *E. coli phoS* gene was generously provided by M. R. Webb (National Institute for Medical Research, London, U.K.). The mutated *phoS* gene was subcloned into a pET28b(+) expression vector using standard molecular biology techniques. The resulting plasmid (pET-PBP) was transformed into

dx.doi.org/10.1021/bi500558d | *Biochemistry* 2014, 53, 5647−5660

chemically competent *E. coli* BL21(λDE3) cells, plated on LB-kan agar, and incubated overnight at 37 °C. Twenty milliliters of LB-kan (34 μg/mL) was inoculated with a single colony and incubated overnight at 37 °C. Ten milliliters of this culture was used to inoculate two 1 L LB-amp flasks. The liquid cultures were incubated, being shaken at 37 °C to midlog phase (A_{600} ∼ 0.7). The cultures were cooled to 18 °C prior to induction with 0.2 mM IPTG. These induced cultures were incubated, shaken at 18 °C for ∼20 h, and harvested by centrifugation. Bacterial cell pellets containing expressed A197C mutant phosphate binding protein (PBP) were resuspended in 100 mL of buffer containing 20 mM Tris-HCl, 500 mM NaCl, 5 mM imidazole, and 10% glycerol (pH 8.0) at 4 °C. Lysis was accomplished when samples were passed through an EmulsiFlex-C5 instrument (Avestin, Inc.) at ∼16000 psi. The lysate was clarified by centrifugation at ∼32500*g* and the supernatant loaded onto ∼3 mL of Ni-agarose resin. The column was washed with >100 column volumes (CV) of lysis buffer, followed by 100 mL of lysis buffer containing 1 M NaCl and then 50 mL of lysis buffer containing 20 mM imidazole. The protein was eluted in buffer containing 20 mM Tris-HCl, 200 mM NaCl, 150 mM imidazole, and 10% glycerol (pH 8.0) at 4 °C. Dithiothreitol (DTT) was added to the pooled protein to a final concentration of 1 mM. The reduced protein was dialyzed versus 1 L of 20 mM Tris, 200 mM NaCl, and 10% glycerol (pH 8.0) at 4 °C overnight. The protein was exchanged into fresh buffer and dialyzed for an additional 4 h. The concentration of the recovered protein was determined spectrophotometrically using an extinction coefficient (ε_{280} = 60880 M^{-1} cm^{-1}) calculated from the deduced protein composition.

PBP was treated for 2 h at room temperature with steady mixing with an "enhanced" phosphate mop prior to being labeled. The mop consisted of 7-methylguanosine (7-MG, 1 mM), purine nucleoside phosphorylase (PNPase, 0.5 unit/mL), phosphodeoxyribomutase (PDRM, 0.02 mg/mL), glucose 1,6-bisphophate (G 1,6-BP, 56 μM), and $MnCl_2$ (1 mM). The "mopped" PBP was reacted with a 1.5-fold molar excess of 7-diethylamino-3-[*N*-(2-maleimidoethyl)carbamoyl]coumarin (MDCC) for 1.5 h at room temperature (constant mixing). The labeled protein was passed over a Ni-NTA column and washed with lysis buffer until the free MDCC was removed. Labeled protein was eluted with elution buffer [20 mM Tris, 200 mM NaCl, 150 mM imidazole, and 10% glycerol (pH 8.0) at 4 °C]. The eluted protein was dialyzed versus 2 L of 20 mM Tris-HCl, 200 mM NaCl, and 20% glycerol (pH 8.0) at 4 °C. The concentration of the labeled protein was determined spectrophotometrically using the calculated extinction coefficient corrected to the absorbance contribution of the label ($0.164\varepsilon_{430} + \varepsilon_{280}$). Labeling efficiency was determined by measuring the absorbance of the label at 430 nm (ε_{430} = 46800 M^{-1} cm^{-1}). The average labeling efficiency was >85%.

Preparation of the Fluorescent Sensor for ADP. Plasmid pJSC1-ParM (His6/I27C/K33A/T174A/T175N/C287A) was also generously provided by M. R. Webb (National Institute for Medical Research). The expression and purification of ParM was essentially the same as for PBP with the exception of ampicillin being the selection antibiotic. Following elution, the concentration was determined spectrophotometrically using an extinction coefficient (ε_{280} = 34380 M^{-1} cm^{-1}) calculated from the deduced protein composition.

Purified ParM was treated with DTT to a final concentration of 1 mM. The reduced protein was dialyzed versus 2× 1 L of 20 mM Tris, 200 mM NaCl, and 10% glycerol (pH 8.0) at 4 °C. The reduced, dialyzed protein was reacted with a 1.5-fold molar excess of MDCC. The reaction was performed at room temperature (RT) for 1.5 h (constant mixing). The labeled protein was passed over a Ni-NTA column and washed with lysis buffer until the free MDCC was removed. Labeled protein was eluted with elution buffer [20 mM Tris, 200 mM NaCl, 150 mM imidazole, and 10% glycerol (pH 8.0) at 4 °C]. The eluted protein was dialyzed versus 2 L of 20 mM Tris-HCl, 200 mM NaCl, and 20% glycerol (pH 8.0) at 4 °C. The concentration of the labeled protein was determined spectrophotometrically using the calculated extinction coefficient corrected to the absorbance contribution of the label [(MDCC coupled to DTT) ε_{280} = 7470 M^{-1} cm^{-1} + $\varepsilon_{280,ParM}$]. The labeling efficiency was determined by measuring the absorbance of the label at 430 nm (ε_{430} = 46800 M^{-1} cm^{-1}). The average labeling efficiency was >90%.

Single-Turnover/Pre-Steady State Analysis of Rad50–MR Complex ATPase Activity. Rapid quench (Bio-Logic, QFM 400) was used to measure the hydrolysis of ATP by Rad50 under single-turnover conditions. Forty microliters of syringe 1 (50 mM Tris-HCl, 0.1 mg/mL BSA, 2 mM $MgCl_2$, 45 μM ATP, and 10 nM ATPγ^{32}P) was rapidly mixed with 20 μL of syringe 2 (50 mM Tris-HCl, 150 mM KCl, 0.1 mg/mL BSA, and 200 μM Rad50) and aged for various times ranging from 0.1 to 3 s and quenched with 20 μL of 10 N formic acid. For longer time points (5−150 s), hand mixing was employed. For reaction mixtures containing Mre11, 30 μL of syringe 1 (50 mM Tris-HCl, 0.1 mg/mL BSA, 2 mM $MgCl_2$, 120 μM ATP, and 10 nM ATPα^{32}P) was rapidly mixed with 15 μL of syringe 2 (50 mM Tris-HCl, 75 mM KCl, 0.1 mg/mL BSA, 30 μM Rad50, and 33 μM Mre11) and aged for various times ranging from 0.1 to 4 s and quenched with 15 μL of 10 N formic acid. For longer time points (5−120 s), hand mixing was employed. The zero time points were accomplished by mixing the protein with the formic acid prior to the addition of ATP. Five microliters of the quenched reaction mixture was spotted onto polyethylenimine (PEI) cellulose TLC plates (20 cm × 20 cm, EMD Chemicals, Inc.). ATP and inorganic phosphate (Rad50) or ADP (MR complex) were resolved using 300 mM potassium phosphate (pH 7.0) as the mobile phase. Following exposure of a phosphor imaging screen to the dried plates, the reaction was visualized using a Typhoon 9410 Variable Mode Imager (Amersham Pharmacia Biotech). The data were analyzed using ImageJ (National Institutes of Health, Bethesda, MD). The hydrolyzed inorganic phosphate (Rad50) or ADP (MR complex) was normalized to the total signal. The percent hydrolysis was plotted as a function of time and the exponential determined using Sigmaplot 10.0 (Systat Software, Inc.). The data analyzed consisted of four separate time courses conducted on two different days for Rad50 and two individual time courses conducted on the same day for the MR complex [an additional time course was conducted for the MR complex at a saturating ATP concentration (500 μM)].

To follow the ATPase reaction for the MR-D complex, DNA was added to 300 μL of the MR complex (50 mM Tris-HCl, 0.1 mg/mL BSA, 21.5 μM Rad50, and 26 μM Mre11) just prior to loading syringe 2. The initial two shots were used to clear the lines prior to data collection. Twenty-five microliters of MgATP (50 mM Tris-HCl, 0.1 mg/mL BSA, 4 mM $MgCl_2$, 500 μM ATP, and either 6 nM ATPγ^{32}P or 6 nM ATPα^{32}P) was rapidly mixed with 25 μL of the MR-D complex, aged for various times ranging from 5 ms to 1.5 s, and quenched with 50 μL of 10 N

dx.doi.org/10.1021/bi500558d | *Biochemistry* 2014, 53, 5647−5660

formic acid. Each time point consisted of three individual shots collected into the same tube. Final reaction concentrations were 10.1 μM Rad50, 12.2 μM Mre11, 14 μM DNA, 2 mM $MgCl_2$, 250 μM ATP, 0.1 mg/mL BSA, and 57 mM KCl in 50 mM Tris-HCl. The zero time point was accomplished by mixing the MR-D complex with formic acid followed by addition of ATP (done through rapid quench); 1.5 μL of the quenched reaction mixture was spotted onto polyethylenimine (PEI) cellulose TLC plates (20 cm × 10 cm, EMD Chemicals, Inc.). The TLC plates were resolved and visualized as described above. Data presented are the average of three time courses conducted on three separate days.

Pulse−chase experiments for the MR-D complex were conducted under conditions like the pre-steady state conditions with the exception of 50 μL of 10−20 mM unlabeled MgATP was mixed with the ongoing reaction mixture after various aging times (5 ms to 1 s). Following the chase of ∼10 s (∼14 turnovers), 25 μL of 23.6 N formic acid (final concentration of 4.7 N) was added to quench the reaction. The time course was analyzed as described above.

Pre-Steady State Analysis of MR-D ATPase Product Release Rates. The stock ATP (20 mM) was mopped by treatment with pyruvate kinase (PK) and lactate dehydrogenase (LDH) (50 mM Tris-HCl, 2 mM reduced nicotinamide adenine dinucleotide, 2 mM phosphoenolpyruvate, 2 mM KCl, 1 mM $MgCl_2$, 4.4 units of PK, and 6.4 units of LDH) at RT for 30 min (constant mixing). The PK/LDH enzymes were removed by centrifugation through an Amicon Ultracel 10K concentrator. To remove any bound phosphate, PBP-MDCC was pretreated with the "enhanced MOP" (2.4 mM 7-MG, 2.4 units of PNPase, 26 mg of PDRM, 48 μM G 1,6-BP, and 1 mM $MnCl_2$) for 1 h at RT (constant mixing). Using a Bio-Logic stopped-flow apparatus, standard curves for the binding of inorganic phosphate to PBP-MDCC and binding of ADP to ParM-MDCC, in the presence of 50 μM ATP, were generated. The acquisition parameters were as follows: 431 nm excitation, 5 nm bandwidth, 460 nm long pass filter, PMT voltage of 350 V with sampling every 2 ms (8000 points, ∼15 s). Assays included 50 mM Tris-HCl, 0.08 mg/mL BSA, 50 mM KCl, 5 mM $MgCl_2$, 0.057 unit/mL PNPase, 0.3 mM 7-MG, 1 μM Rad50, 1.1 μM Mre11, 1.25 μM DNA substrate, and 5 μM PBP or ParM. Every progress curve analyzed was an average of four individual curves. Because of the binding of ATP to the fluorescent probes (mainly ParM), the reaction data were normalized to a zero protein progress curve. The progress curves were fit to a rapid equilibrium random uni-bi mechanism preceded by a slow complex formation step. The complex formation step and individual product release rates were allowed to float during the fitting process. The script used for fitting the progress curves is presented in Figure S1 of the Supporting Information.

ATPase pH−Rate Profile. The ATPase activity (WT and H536Q) of the MR-D complex was measured as a function of pH. The standard coupled assay was used with the exception of different buffer components. The following buffers (50 mM) were utilized: 2-(4-morpholino)ethanesulfonic acid (MES, pH 5.5−6.5), 2-[4-(2-hydroxyethyl)piperazin-1-yl]ethanesulfonic acid (HEPES, pH 7.0−7.5), 2-amino-2-hydroxymethylpropane-1,3-diol (Tris, pH 8.0−8.5), and *N*-cyclohexyl-2-aminoethanesulfonic acid (CHES, pH 9.0−10.0). The integrity of the coupling enzymes at the extreme pH was verified by the addition of ADP. To ensure that the decrease in activity was truly a function of pH, the complex was preincubated at the extreme pH and then assayed in Tris-HCl (pH 7.6, 30 °C). The specific activity at each pH was determined at least seven times over 4 days. These data were fit to a bell-shaped curve depicting two pK_a values using the equation $y = V_{maxlim}/(1 + 10^{pK_a - pH} + 10^{pH - pK_b})$ [Sigmaplot 10.0/Enzyme Kinetics Module 1.3 (Systat Software, Inc.)].

Determination of DNA Equilibrium Dissociation Constants for WT and Mutant Rad50s. The dsDNA binding properties of Rad50 were monitored using a Synergy 2 Multi-Mode microplate reader. All assays were conducted at ambient temperature in the presence of 10 nM hexachlorofluorescein-labeled DNA substrate. Binding assays were conducted in the presence of 50 mM Tris-HCl, 50 mM KCl, 5 mM $MgCl_2$, and 0.1 mg/mL BSA (pH 7.6). The protein concentration ranged from 0 to 12 μM. Samples were excited at 520 nm, and polarization was followed at 560 nm. Data (collected in triplicate) were fit to a simple binding isotherm with a background correction: $y = (B_{max}[x])/(K_d + [x]) + c$ (Sigmaplot 10.0).

Deuterium Solvent Isotope Effect on ATPase Activity. The ATPase specific activity of WT and mutant Rad50s in the absence or presence of Mre11 and DNA was determined in either aqueous 100 mM Tris-HCl buffer (pH 7.6) or 100 mM Tris deuterium oxide (pH 8.0). To account for the difference in the ionization constants for groups in H_2O versus D_2O, the "cancel-out" approach was used to determine the appropriate pH for the D_2O comparison (pH = pD − 0.4).[21] Rad50, Mre11, and DNA concentrations varied depending upon the activity of each mutant. The ATP concentration was at least $5S_{0.5}$, with the exception being that of S43A Rad50 ($2S_{0.5}$). $MgCl_2$ was always kept in excess of ATP. To minimize sample variation, 30 μL of Rad50 (or MR-D) was mixed with 30 μL of a solution containing KCl, PEP, ATP, $MgCl_2$, and PK/LDH. Twenty-five microliters of this reaction mixture was added to either 700 μL of aqueous 100 mM Tris-HCl (7.6) or 700 μL of 100 mM Tris-HCl in deuterium oxide (8.0; final D_2O concentration of 86.7%). The final concentrations of components were 50 mM KCl, 259 μM PEP, 159 μM NADH, 1 unit of PK, and 1.6 units of LDH. The reactions were monitored simultaneously in a Cary Eclipse fluorescence spectrometer. The data presented are the average of three individual reactions (each individual reaction consisted of two aqueous and two deutero samples).

Effect of Viscosity on ATPase Activity. Viscosity experiments were conducted with sucrose [0−30% (w/v)] and Ficoll-400 [0−10% (w/v)]. The relative viscosity was determined using a Cannon-Fenske 50 viscometer (Sigma-Adrich) and calculated using the formula $\eta_{rel} = (t/t^\circ)(\rho/\rho^\circ)$.[22] The variables t° and ρ° refer to the viscometer efflux time and the density of the assay buffer sans viscogen, respectively. All densities were determined gravimetrically. Efflux times were determined for 0, 5, 15, and 30% (w/v) sucrose. The relative viscosities were plotted as a function of viscogen concentration and fit to an exponential. This exponential was used to determine the relative viscosities of the intermediate concentrations. This was repeated for Ficoll-400 [0, 2.5, and 5.0% (w/v)]. All efflux times used were an average of three measurements. The specific activity of Rad50 and the MR-D complex was determined as described above with the exception of increasing the viscogen concentration.

dx.doi.org/10.1021/bi500558d | *Biochemistry* 2014, 53, 5647−5660

Table 1. Steady State ATPase Kinetic Constants and MgATP Affinities for WT and Mutant Rad50s[a]

protein	$S_{0.5}$ (μM)[b,c]	k_{cat} (s^{-1})[b]	n	K_d (μM)[b]
WT[d]	16 ± 1	0.145 ± 0.003	1.4 ± 0.1	9.4 ± 1.2
S43A[e]	1486 ± 274	0.0048 ± 0.0003	0.94 ± 0.09	331 ± 36
D504N[e]	479 ± 38	0.011 ± 0.001	0.7 ± 0.1	397 ± 56
E505Q	36 ± 46	0.005 ± 0.0002	0.5 ± 0.2	5.6 ± 0.6
H536A	8.2 ± 0.6	0.021 ± 0.001	1.5 ± 0.2	10.1 ± 1.1
H536Q	57 ± 3	0.100 ± 0.003	1.6 ± 0.1	48.6 ± 5.7
E505Q/H536A	nd[g]	0.0018 ± 0.0003[f]	nd[g]	2.7 ± 0.2

[a]Fluorometric assays were performed as described in Materials and Methods. [b]Errors represent the standard error of the fit. [c]$S_{0.5}$ is the ATP concentration at half-maximal velocity, as calculated from a fit of the ATP saturation data to the Hill equation. [d]From ref 18. [e]Assay contained 10 mM $MgCl_2$. [f]Specific activity determination under standard conditions using the same buffer conditions. The error represents the standard deviation of 12 measurements. [g]Not determined.

Table 2. Steady State ATPase Kinetic Constants for WT and Mutant Rad50s in the Presence of Mre11 and DNA[a]

protein	$S_{0.5}$ (μM)[b]	k_{cat} (s^{-1})	n	x-fold activation
WT[c]	49 ± 2	3.2 ± 0.1	2.4 ± 0.2	21.9
S43A	114 ± 28	0.020 ± 0.002	1.1 ± 0.3	4.2
D504N	160 ± 18	0.014 ± 0.001	1.0 ± 0.1	1.8
E505Q	27 ± 1	0.0103 ± 0.0007	1.1 ± 0.2	2.6
H536A	7.8 ± 0.1	0.022 ± 0.001	1.3 ± 0.1	1.0
H536Q	63 ± 4	0.434 ± 0.014	1.8 ± 0.2	4.3
E505Q/H536A	36 ± 5	0.021 ± 0.001	1.05 ± 0.12	11.9

[a]Fluorometric assays were performed as described in Materials and Methods. Errors represent the standard error of the fit. [b]$S_{0.5}$ is the ATP concentration at half-maximal velocity, as calculated from a fit of the ATP saturation data to the Hill equation. [c]From ref 18.

RESULTS

Steady State ATPase Activity. Residues from three of the six ABC protein superfamily motifs were evaluated in this study. All of the mutants studied, with the exception of H536Q, were kinetically perturbed compared to the WT enzyme for Rad50 alone (Table 1). The k_{cat} for the Walker A serine (S43A) mutant was 30-fold lower than the WT value. More interestingly, the Half Saturation constant ($S_{0.5}$) was significantly inflated (93-fold) and the cooperativity abolished (Hill coefficient of 1.0). The two acidic residues of the Walker B-motif also had diminished k_{cat} values upon being mutated (13-fold for D504N and 29-fold for E505Q). Additionally, the $S_{0.5}$ for D504N was increased 65-fold. The Walker B mutants displayed negative cooperativity upon being fit to the Hill equation. The histidine (H536) that defines the H-loop motif was mutated to either an alanine or a glutamine. These mutations were the least affected. The ATP turnover of H536Q was essentially the same as that of WT, whereas that of the alanine mutant was only 7-fold lower. The $S_{0.5}$ for H536Q was modestly inflated (3.6-fold).

The kinetic constants were also determined for these mutants in the presence of Mre11 and DNA (Table 2). The effect on ATP hydrolysis was more pronounced for the MR-D complex than for Rad50 alone. S43A activity was diminished by 160-fold. D504N activity and E505Q activity were decreased by 229- and 311-fold, respectively. The histidine mutants, again, had the weakest effect on activity (154-fold for H536A and 7-fold for H536Q). The WT enzyme is activated by the addition of Mre11 and DNA by ~22-fold. Upon comparison of the fold diminution between Rad50 and the MR-D complex, the H536A mutation had a much more pronounced affect for the MR-D complex (no activation). Surprisingly, the double mutant (E505Q/H536A) displayed one of the highest activations (11.9-fold). The Michaelis constant for S43A and D504N was also inflated for the MR-D complex, but the degree of inflation was much reduced compared to that of Rad50 alone (2.3- and 3.3-fold, respectively). The ATPase activity is highly cooperative for the WT enzyme in the presence of Mre11 and DNA (Hill coefficient of 2.4). Although all of the mutants exhibited a decrease in cooperativity, four mutants (S43A, D504N, E505Q, and H536A) exhibited little to no cooperative behavior.

Determination of MgATP and DNA Dissociation Constants of Mutant Rad50s. The dissociation constants for MgATP were determined to discern the degree to which MgATP affinity contributed to the inflated $S_{0.5}$. The two mutants that had inflated Half Saturation constants ($S_{0.5}$) for MgATP [S43A and D504N (Table 1)] also displayed inflated K_d-MgATP values that were similar in magnitude (35- and 42-fold, respectively). The K_d-MgATP values of the remaining mutations also tracked well with their Half Saturation constants ($S_{0.5}$).

The K_d-DNA was determined for WT Rad50 by following the fluorescent polarization of hexachlorofluorescein-labeled DNA. The WT affinity for DNA was estimated to be 198 nM (Table 3). All of the mutants exhibited similar K_d-DNA estimates (<2-fold), suggesting that the mutations did not affect binding to DNA.

Pre-Equilibrium Tryptophan Quenching upon MgATP Binding. In the process of determining the on and off rates for MgATP binding, we observed that the relationship between MgATP concentration and the rate of tryptophan quenching was nonlinear (Figure 1, inset). This nonlinearity was suggestive of a conformational change following MgATP binding becoming rate-limiting. To explore these data, the progress curves were globally fit to a simple binding mechanism followed by a conformational change (Figure 1). This yielded four microscopic rate constant estimates corresponding to the on and off rates [k_1 and k_2, respectively (Table 4)] and the forward and reverse rates of the conformational change [k_3 and k_4, respectively (Table 4)]. An alternative mechanism that

dx.doi.org/10.1021/bi500558d | Biochemistry 2014, 53, 5647−5660

Table 3. Equilibrium Dissociation Constants for Binding of DNA to WT and Mutant Rad50 Proteins[a]

protein	K_d (nM)	B_{max}
WT	198 ± 16	252 ± 5
N38A	126 ± 12	255 ± 6
S43A	331 ± 36	266 ± 7
D504N	241 ± 18	241 ± 5
E505Q	264 ± 28	244 ± 6
D512N	248 ± 34	234 ± 7
H536A	381 ± 47	233 ± 7
H536Q	372 ± 37	237 ± 5
E505Q/H536A	96 ± 10	244 ± 6

[a]The dsDNA binding properties of Rad50 were determined as described in Materials and Methods.

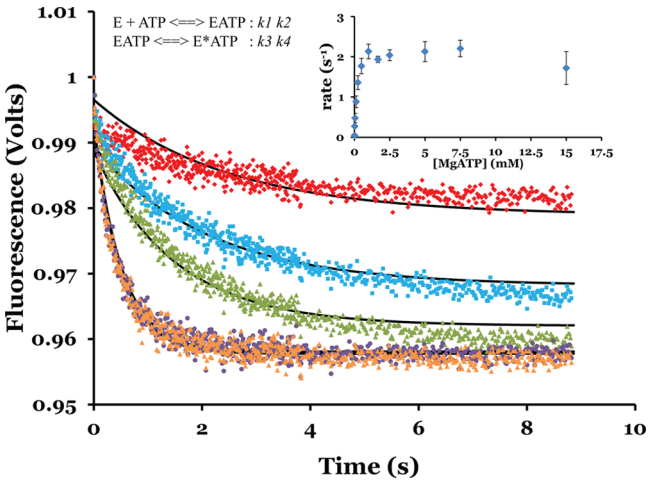

Figure 1. Conformational change prior to chemistry is not rate-limiting for Rad50 ATPase activity. The rate of tryptophan quenching was determined at 12 ATP concentrations [from 17 μM to 15 mM (inset)]. Because of nonlinearity, these data were globally fit to the mechanism described above using Dynafit3 (Biokin, Ltd.[20]). Five representative curves [17 μM (red diamonds), 25 μM (blue squares), 50 μM (green triangles), 2.5 mM (purple circles), and 7.5 mM ATP (orange triangles)] are depicted. All microscopic rate constants were allowed to float in the simulation.

Table 4. Rate Constant Estimates for the Binding of MgATP to WT Rad50

rate constant	value[a]	SD[b]
k_1 (μM^{-1} s^{-1})	18.1	8.5
k_2 (s^{-1})	2629	303
k_3 (s^{-1})	1.5	0.3
k_4 (s^{-1})	0.19	0.03

[a]The rate constant estimates reported are the average of three sets of MgATP titrations with MgATP concentrations ranging from 17 μM to 15 mM. The individual data sets were fit to the mechanism shown in Figure 1 using DynaFit3 (Biokin, Ltd.[20]). [b]The errors represent the standard deviation of the three sets.

included a chemical step following the conformational change was also tested and did not significantly improve the fit. Using the estimates from the mechanism without a chemical step, the calculated kinetic K_d (18.4 ± 10.0 μM) was in good agreement with the equilibrium K_d previously determined (9.4 ± 1.2 μM[17]).

pH−Rate Profile for WT and H536Q Rad50 in the Presence of Mre11 and DNA. The specific activity of the WT and H536Q MR-D complex was determined over the pH range of 5.5−10 (Figure 2). These data were fit to a bell-shaped

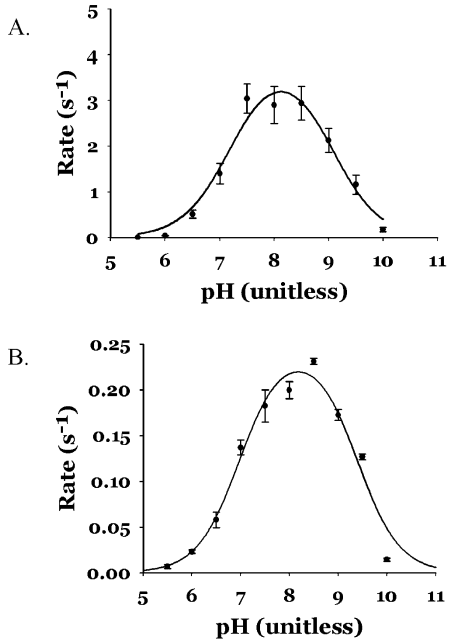

Figure 2. ATPase activity of Rad50 in the presence of Mre11 and DNA as a function of pH. pH−rate profiles for the hydrolysis of ATP by the WT complex (A) and the H536Q Rad50−WT Mre11 complex (B). These data were fit to a bell-shaped curve depicting two pK_a values using the equation $y = V_{maxlim}/(1 + 10^{pK_a - pH} + 10^{pH - pK_b})$ (Sigmaplot 10.0/Enzyme Kinetics Module 1.3).

curve characterized by two pK_a values. Both WT (7.2 ± 0.1 and 9.1 ± 0.1) and H536Q (7.0 ± 0.1 and 9.4 ± 0.1) had similar pK_a estimates, arguing against H536Q acting as a catalytic base. The pK_a of ∼9 is likely attributed to the Walker A lysine (K42) that stabilizes the negative charge that is expected to form during the transition state. It has been shown that removal of the positive charge by mutation of this residue to methionine decreased the ATPase specific activity of the MR-D complex by ∼4000-fold.[18] Unfortunately, the E505Q mutation was unstable (precipitation) at pH <7.5 and could not be evaluated further.

Evaluation of Nuclease Activity. Nuclease activity was monitored by the liberation of the fluorescent base analogue, 2-aminopurine (2AP), from either position 1 or position 17 relative to 3′ end. 2-AP has little fluorescence when it is involved with a base-stacked partner; this fluorescence is greatly enhanced when the base stacking is removed.[23] The nuclease rate was estimated for the MR complex with the 2-AP at position 1 in the presence and absence of ATP (Table 5). In the absence of ATP, the WT complex excised the 2-AP at a rate of 6.8 ± 1.6 min^{-1}. All of the mutants tested had activity similar to that of WT (<2-fold). The nuclease activity was slightly depressed in the presence of ATP (4.62 ± 0.38 min^{-1} for WT). All of the mutants also had lower nuclease activity with ATP, similar to the WT enzyme (<3-fold). It has been previously shown that processive nuclease activity is ATP-dependent.[17] Therefore, the WT and mutant MR complex nuclease activities were estimated with the 2-AP probe located at position 17 relative to the 3′ end (Table 6). The WT excised position 17 at

dx.doi.org/10.1021/bi500558d | Biochemistry 2014, 53, 5647−5660

Table 5. Rates of Excision of 2-Aminopurine from Position 1 (relative to the 3′ end, 50-mer) for the Rad50−Mre11 Complex in the Presence and Absence of ATP[a]

protein	rate without ATP (min^{-1})	rate with ATP (min^{-1})[b]
WT	6.80 ± 1.60	4.62 ± 0.38
N38A	9.59 ± 1.05	2.68 ± 0.28
S43A	4.48 ± 0.50	1.75 ± 0.36
D504N	5.63 ± 0.80	2.03 ± 0.30
E505Q	5.68 ± 1.23	3.30 ± 0.35
D512N	8.28 ± 0.96	2.78 ± 0.27
H536A	6.48 ± 1.12	3.13 ± 0.56
H536Q	6.33 ± 1.89	2.64 ± 0.17
E505Q/H536A	7.80 ± 0.84	2.95 ± 0.11

[a]Fluorometric assays were performed as described in Materials and Methods. Errors represent the standard deviation of at least six replicates. [b]The ATP concentration was fixed at 2.5 mM.

Table 6. Rates of Excision of 2-Aminopurine from Position 17 (relative to the 3′ end, 50-mer) for the Rad50−Mre11 Complex in the Presence of ATP[a]

protein	rate (min^{-1})
WT	0.25 ± 0.05
N38A[b]	0.005 ± 0.001
S43A	0.005 ± 0.001
D504N	0.019 ± 0.004
E505Q	0.080 ± 0.044
D512N[b]	0.006 ± 0.001
H536A	0.058 ± 0.022
H536Q	0.055 ± 0.012
E505Q/H536A	0.054 ± 0.010

[a]Fluorometric assays were performed as described in Materials and Methods. Errors represent the standard deviation of at least six replicates. [b]From ref 22.

a rate of 0.25 ± 0.05 min^{-1}. Most of the mutations resulted in a modest decrease (~5-fold) in processive nuclease activity. Interestingly, three of the mutants (N38A, S43A, and D512A) that were significantly affected (~50-fold decrease in activity) are all associated with the Walker A-motif and similar in magnitude to the diminution of the only other Walker A mutation (31-fold for K42M).[18,24]

Determination of the ATPase Reaction Rate-Limiting Step for Rad50, MR, and the MR-D Complex. The Rad50 ATPase reaction was followed under single-turnover conditions using a quenched-flow apparatus. At the ATP concentration used in the experiment (30 μM), the calculated rate based on the determined steady state constants is 0.11 s^{-1}. The average rate measured was 0.061 s^{-1}, suggesting that chemistry or a preceding step is rate-limiting (Figure 3A).

The $S_{0.5}$-ATP for the MR complex (42 μM) is elevated compared to that of Rad50 alone (16 μM). Maintaining conditions for single turnover similar to those used with Rad50 alone requires relatively high concentrations of proteins (183 μM complex in the shot and 549 μM complex in the syringe). Unfortunately, the proteins are not stable at these concentrations (possibly because of the extended coiled-coil domain of Rad50). Therefore, a pre-steady state approach was taken to explore the rate-limiting step for the MR complex as lower concentrations are required for these experiments. The time course is linear without a burst phase (*y*-intercept of 0.5 μM), and the measured rate (0.145 s^{-1}) correlates well with the calculated steady state rate (0.164 s^{-1}), again suggesting that chemistry or a preceding step is rate-limiting (Figure 3B). Similar results were obtained when the reaction of the pre-steady state MR (10 μM) complex was repeated using a saturating ATP concentration (500 μM). The time course was linear with a steady state rate of 0.254 s^{-1} (k_{calc} = 0.221 s^{-1}) with a *y*-intercept of 2.2 μM.

A pre-steady state approach was also used to probe the rate-limiting step of the MR-D complex at saturating concentrations of ATP (5-fold $S_{0.5}$, 250 μM). When the specific activity of the MR-D complex was determined using the standard enzyme-coupled assay, the complex retained only 50% of the original activity determined prior to the time course. Considering the MR complex was stable at the same concentration (10 μM), addition of DNA appears to result in an unstable complex. Because of this issue, DNA was added to a small volume (300 μL) of the MR complex just prior to loading the rapid quench syringe. This volume was sufficient to obtain two time points. Additionally, to increase the stability of the complex, the temperature was reduced to 25 °C. Only time courses that exhibited a steady state rate that was at least 75% of the rate determined prior to the time course (2.0 s^{-1}) were included in the analysis. On four consecutive days, only one failed to meet this criterion. The entire time course was then fit to a linear regression, and on the basis of this analysis, a rate of 1.59 ± 0.08 s^{-1} was determined with a *y*-intercept of 2.8 ± 0.4 μM (Figure 3C, solid line). These data argue against any noticeable burst; however, the noise at very short time points (5−100 ms) could be obscuring a small amplitude burst. To test for this possibility, we included only the later time points (250 ms to 1.5 s) in the linear regression fit (Figure 3C, dotted line). This resulted in a rate of 1.80 ± 0.13 s^{-1} with a *y*-intercept of 0.6 ± 1.2 μM. This analysis indicates the absence of a pre-steady state burst and suggests that chemistry is rate-limiting for the MR-D complex, as well.

To confirm the rapid binding of ATP, a pulse−chase experiment was performed. The experiment was performed like the pre-steady state determination with the exception of the aged reaction (5 ms to 1 s) being "chased" with 10 or 20 mM unlabeled MgATP for 10 s (~14 turnovers) and then quenched via the addition of formic acid. The MR-D complex (10 mM) appears to bind and hydrolyze one molecule of the ATP−Rad50 monomer (Figure 4D, amplitude of 7.6 μM) within the first time point (5 ms), suggesting an apparent diffusion-limited binding rate (>10^7 M^{-1} s^{-1}). To increase our level of confidence in the presence of a rapid burst, again only the later time points (250 ms to 1.5 s) were included in a linear regression fit. The measured rate from this analysis was 1.6 ± 0.1 s^{-1} with a *y*-intercept of 11.6 ± 0.6 μM.

Considering the complications with high concentrations of the MR-D complex (i.e., instability), we also employed an indirect fluorescence method that does not require high protein concentrations. The rates of product release (ADP and inorganic phosphate) were measured by rapid kinetics using the fluorescent biosensors for these metabolites (PBP, P_i; ParM, ADP). Because these probes detect product after their release from the enzyme, a burst phase is expected only if the release of one product is rate-limiting (but not simultaneous release of both). Visual inspection of the time courses (Figure 4) revealed a minor but noticeable lag period, which is then followed by a linear phase before the probes become saturated (Figure 4). Although the probe concentration was 5 μM, the PBP saturated at a concentration of 4.3 μM, which is likely due

dx.doi.org/10.1021/bi500558d | *Biochemistry* 2014, 53, 5647−5660

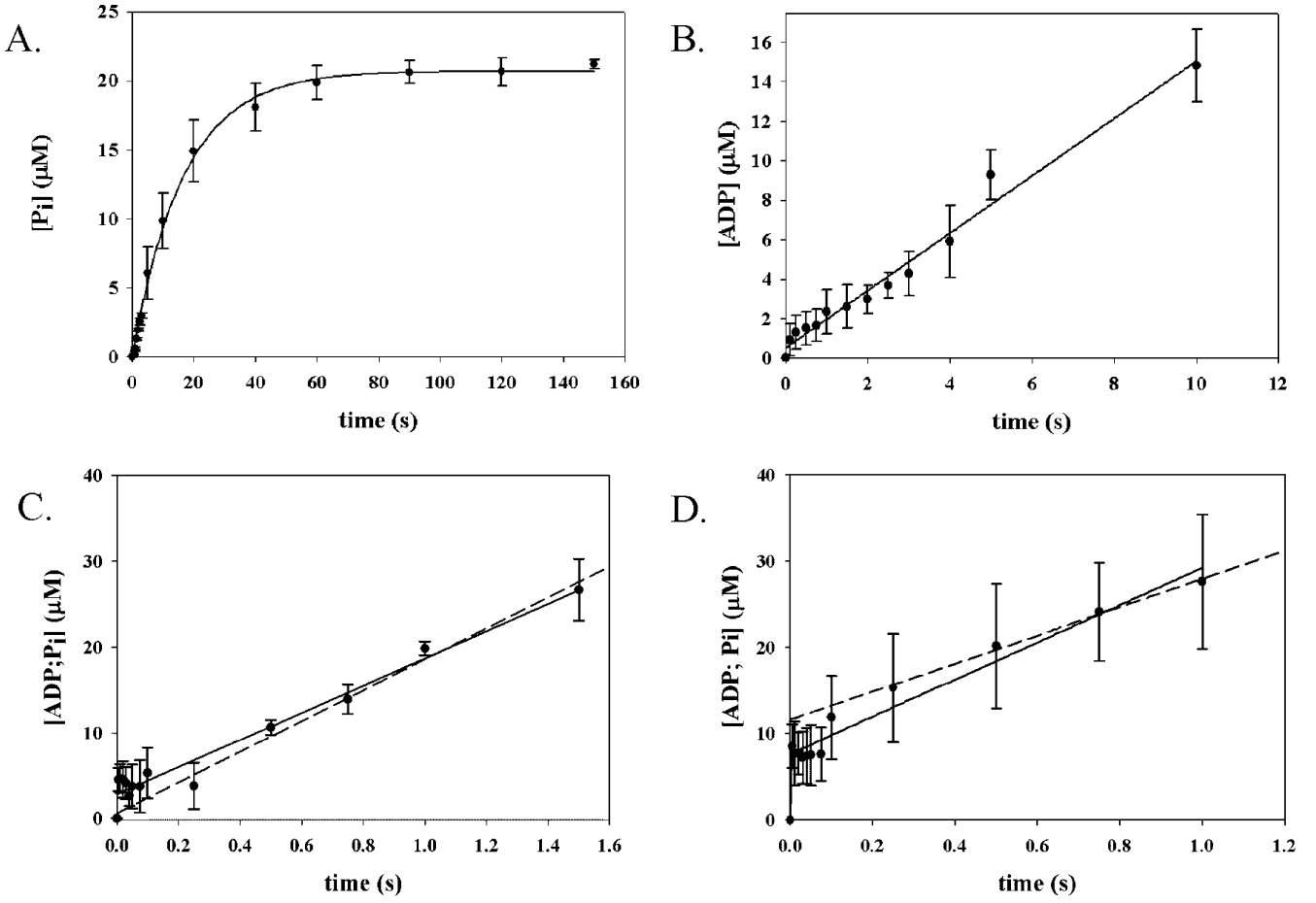

Figure 3. Chemistry or preceding step is rate-limiting for Rad50 and the Rad50−Mre11 complex. (A) Rad50 ATPase activity under single-turnover conditions at 67 μM Rad50 and 30 μM [MgATP. The calculated rate was 0.110 s^{-1} and the measured rate 0.060 s^{-1}. (B) Pre-steady state ATPase activity of the Rad50−Mre11 complex at 10 μM complex and 80 μM MgATP. The calculated rate was 0.164 s^{-1} and the measured rate 0.145 ± 0.007 s^{-1} with a *y*-intercept of 0.53 ± 0.26 μM. (C) Pre-steady state ATPase activity of the Rad50−Mre11 complex in the presence of DNA at 10 μM MR-D and 250 μM MgATP. The calculated rate was 3.2 s^{-1} and the measured rate (—) 1.6 ± 0.1 s^{-1} with a *y*-intercept of 2.8 ± 0.4 μM. The dotted line shows a regression fit to the later time points (250 ms to 1.5 s), with a measured rate of 1.8 ± 0.1 s^{-1} with a *y*-intercept of 0.56 ± 1.22 μM. (D) Pulse−chase analysis of the Rad50−Mre11 complex in the presence of DNA. The MR-D (10 μM) complex appears to bind one molecule of the ATP−Rad50 monomer (amplitude of 7.6 μM) within the first time point (5 ms), suggesting an apparent diffusion-limited binding rate (>10^7 M^{-1} s^{-1}). The dotted line shows a regression fit to the later time points (250 ms to 1.5 s), with a measured rate of 1.6 ± 0.1 s^{-1} with a *y*-intercept of 11.6 ± 0.6 μM.

to residual P_i that has not been completely removed by the phosphate "MOP". The lack of a burst phase in both time courses indicates that either chemistry or a preceding step is rate-limiting or that ADP and P_i are released in a concomitant fashion. However, because the lag period could obscure a potential burst phase, we performed kinetic simulations (Dynafit3, Biokin, Ltd.[20]) to confirm that even a 1.5−2-fold difference in product release rates should be visually apparent (data not shown). We then simultaneously fit these two independent time courses to a rapid equilibrium random uni-bi mechanism that included a slow complex formation step using Dynafit3 (Biokin, Ltd.[20]). To demonstrate that the release of a single product (ADP or P_i) was not was not rate-limiting, the chemical step was fixed at 100 s^{-1} (i.e., not limiting), while the product off rates and the rate of complex formation were allowed to float. To ensure the product release rates were well determined and not correlated, the data were fit twice using different initial estimates of the product release rates (fit 1, ADP off rate estimated to be 10 times the estimate of the P_i off rate; fit 2, P_i off rate estimated to be 10 times the estimate of the ADP off rate). The analysis provided a rate constant for complex formation of 2.82 ± 0.04 s^{-1} ($t_{1/2}$ of 246 ms) and product release rates for ADP and P_i of 1.93 ± 0.01 and 2.21 ± 0.02 s^{-1}, respectively. Because the release rates of ADP and P_i are essentially identical, the rate-limiting step of the MR-D ATPase reaction is either the concomitant release of products or a step prior to product release (i.e., chemistry).

Effect of Increasing Solvent Viscosity on ATPase Reaction Rate. To further confirm that chemistry or a preceding step is rate-limiting, as opposed to product release, the ATPase reaction was monitored for Rad50 and the MR-D complex in the presence of an increasing viscogen concentration. It has been shown that macroviscogens do not affect the rates of diffusion of small molecules; instead, they affect the "bulk properties" of a system unrelated to small molecule diffusion.[25,26] Microviscogens do affect the diffusional rate of small molecules, such as enzyme substrates and products into and out of the active site, or the bulk properties of the system.[25,26] To distinguish between whether any effect observed was caused by a decreased rate of diffusion of the

dx.doi.org/10.1021/bi500558d | *Biochemistry* 2014, 53, 5647−5660

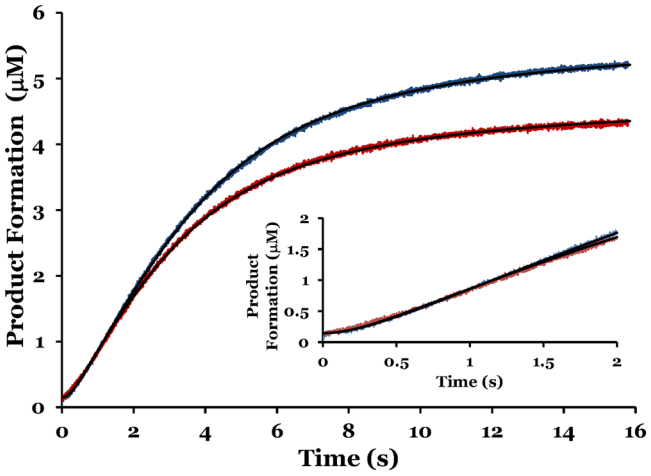

Figure 4. ATPase activity of Rad50 in the presence of Mre11 and DNA under pre-steady state conditions. ATPase activity was monitored by following product release of ADP using the fluorescent sensor, ParM (blue trace), or release of inorganic phosphate using the fluorescent sensor, PBP (red trace). Assays included 1 μM Rad50, 1.1 μM Mre11, 1.25 μM DNA, and 50 μM MgATP. Progress curves fit to a rapid equilibrium random uni-bi mechanism preceded by a slow assembly step using Dynafit3 (Biokin, Ltd.[20]; mechanism presented in the Supporting Information).

product or nonspecific effects, the reaction was followed using both a microscopic viscogen (sucrose) and a macroscopic viscogen (Ficoll-400). Increasing the concentration of sucrose had no effect on the reaction rate for Rad50 (slope = 0.0079; R^2 = 0.0292) or Rad50 in the presence of Mre11 (slope = 0.0304; R^2 = 0.3106) (Figure 5B). The effect of increasing the concentration of Ficoll-400 on the reaction rate for Rad50 (slope = 0.1319; R^2 = 0.9714) and Rad50 in the presence of Mre11 (slope = 0.0887; R^2 = 0.9568) (Figure 5, panel B) was minimal. Increasing the concentration of sucrose had a minor effect on the reaction rate of the MR-D complex (slope = 0.3989; R^2 = 0.9713) (Figure 5A). There was also a minor effect on the reaction rate caused by increasing the concentration of Ficoll-400 (slope = 0.2276; R^2 = 0.9680) (Figure 5A). These data coupled with the single-turnover and pre-steady state data strongly suggest that product release is not rate-limiting for Rad50, Rad50 in the presence of Mre11, or the MR-D complex. The lack of a strong microviscosity effect is consistent with a rapid equilibrium mechanism.

Deuterium Solvent Isotope Effect. The experiments thus far strongly suggest that chemistry is the rate-limiting step of Rad50 and the MR-D complex. To elucidate if the ATPase reaction is associative or dissociative in nature, the specific activity was determined in D_2O for Rad50 and the MR-D complex (Table 7). The WT protio to deutero rate ratio was near unity (0.92 for Rad50 and 0.98 for MR-D). The Rad50 reaction rate ratio for the mutants was similar to that of the WT enzyme. For the MR-D complex, the mutant ratio ranged from unity to slightly inverse (0.82 for S43A, 0.88 for D504N, 0.79 for E505Q, 0.96 for H536Q, 0.88 for H536A, and 0.73 for E505Q/H536A). These data argue against a catalytic base being involved and for the reaction to proceed by a dissociative mechanism.

DISCUSSION

The Rad50–Mre11 complex is essential for the repair of double-strand breaks in DNA, and homologues exist in all

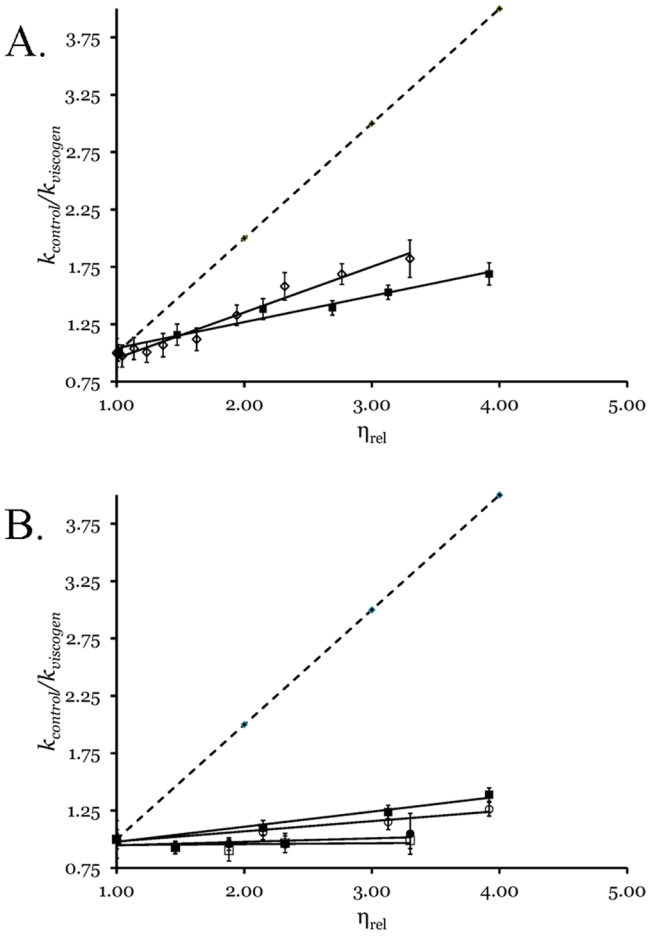

Figure 5. Effect of solution viscosity on ATP hydrolysis. (A) Plot of $k_{control}/k_{viscogen}$ of the MR-D complex vs relative viscosity: sucrose (◇) and Ficoll-400 (■). (B) Plot of Rad50 [sucrose (□) and Ficoll-400 (■)] and Rad50 in the presence of Mre11 [sucrose (●) and Ficoll-400 (○)] as a function of viscosity. The dashed line represents product release being completely rate-limiting (slope = 1).

Table 7. Deuterium Solvent Isotope Effect on ATP Turnover for WT and Mutant Rad50 in the Absence and Presence of WT Mre11 and DNA[a]

protein	k_{H_2O}/k_{D_2O}[b]	k_{H_2O}/k_{D_2O}[c]
WT	0.92 ± 0.05	0.98 ± 0.05
S43A	0.96 ± 0.11	0.82 ± 0.10
D504N	0.88 ± 0.04	0.64 ± 0.08
E505Q	1.14 ± 0.06	0.79 ± 0.02
H536Q	0.97 ± 0.02	0.79 ± 0.05
H536A	0.88 ± 0.02	0.78 ± 0.01
E505Q/H536A	0.73 ± 0.08	0.77 ± 0.04

[a] k_{H_2O} is the reaction rate determined in Tris (100 mM, pH 7.6)-buffered H_2O; k_{D_2O} is the reaction rate determined in Tris (100 mM, pH 8.0)-buffered D_2O. The D_2O concentration was 86.9%. [b] Deuterium isotope effect for Rad50. [c] Deuterium isotope effect for Rad50 in the presence of WT Mre11 and DNA.

kingdoms of life.[27] Obtaining large quantities of the prokaryotic, eukaryotic, and archaeal complex has proven difficult, presumably because of the large coiled-coil region of the Rad50 homologues. We have developed a robust expression system for the bacteriophage T4 Rad50 and Mre11[18] and characterized the WT steady state ATPase/nuclease kinetics

dx.doi.org/10.1021/bi500558d | Biochemistry 2014, 53, 5647–5660

and functionally evaluated residues in the ABC-defining signature motif and D-loop motifs.[17,18] In this report, we functionally characterize residues in the Walker A/B- and H-loop motif with the goal of defining the mechanism of ATP hydrolysis. We have also identified the rate-limiting step for Rad50, the MR complex, and the MR-D complex.

Steady State ATPase Kinetics. Proteins belonging to the ABC protein superfamily are characterized by six conserved motifs.[28] Although mutations in the consensus motifs have been phenotypically characterized (mainly measuring rates of transport[29,30]), a careful evaluation of ATPase kinetics has just begun. We have recently characterized the WT bacteriophage T4 MR-D complex,[18] as well as residues in the signature motif,[17] the D-loop aspartate, and Walker A asparagine.[24] In this study, the remaining motif residues have been mutated and ATPase kinetic characterization has been performed.

Walker A Serine and Walker B Aspartate: MgATP Binding and Catalysis. The Walker A-motif is generally characterized by the sequence "GXXXXGK(T/S)".[12,31] Recently, the Walker A serine was mutated in the human multidrug resistance-associated protein, MRP1.[32] Yang et al. qualitatively showed the S1334A mutation displayed decreased affinity for MgATP and impaired catalysis. The S1334A mutant also decreased the level of leukotriene C4 (LTC4) transport (<10% of the WT value). We have taken a more quantitative approach to evaluating the corresponding mutation. In the crystal structure of the *Pyrococcus furiosus* Rad50, the Walker A serine is directly coordinated to the magnesium of the MgATP substrate and the Walker B aspartate [Protein Data Bank (PDB) entry 3QKT[15]]. Not surprisingly, mutation of this residue to an alanine substantially decreases the affinity for MgATP (35-fold) compared to that of WT Rad50, as well as a decreased rate of turnover (30-fold), suggesting this mutation drastically perturbs the structure of the active site. We have previously argued that Rad50 follows a rapid equilibrium mechanism;[17] if this holds true for the MR-D complex, the addition of Mre11 and DNA to S43A Rad50 promotes a conformation more productive to MgATP binding (inflation in $S_{0.5}$ of only 2.3-fold). These data suggest that the Walker A terminal hydroxyl is important not only in structuring the active site for binding MgATP but also in orienting the substrate for efficient hydrolysis.[33]

The Walker B-motif is characterized by the sequence "hhhhDE".[34] The Walker B aspartate has previously been characterized in the yeast ATP binding cassette transporter.[29] Falcon-Perez et al. showed the D777N mutation increased the Half Saturation constant ($S_{0.5}$) for MgATP (28-fold). Surprisingly, the effect on LTC4 transport was only minimally perturbed (2.6-fold). Again, consulting the crystal structure of *P. furiosus* Rad50 (PDB entry 3QTK,[15]), we found the aspartate is coordinating a water molecule in the first coordination sphere of the Mg^{2+} and hydrogen-bonded to the Walker A serine. Not surprisingly, the D504N kinetic constants are similar to those of the S43A and D777N mutations in Ycf1p. MgATP affinity is decreased by ∼42-fold for Rad50, and hydrolysis is similarly impaired (18-fold). The addition of Mre11 and DNA, again, promoted a more productive complex in terms of both MgATP affinities.

Elucidation of the Rate-Limiting Step. The rate-limiting step has been determined for only a few ABC ATPase proteins. MutS, an ABC ATPase belonging to the SMC family of proteins, is one of the few to be investigated. Bjornson et al. showed burst activity in pre-steady state experiments for MutS alone and MutS in the presence of homoduplex DNA. On the basis of these data, they concluded product release is rate-limiting.[35] Interestingly, when the reaction was conducted in the presence of heteroduplex DNA, the burst phase was lost and the rate-limiting step became chemistry or a preceding step. Much like the case for MutS in the presence of homoduplex DNA, product release (ADP) is rate-limiting for the *E. coli* ABC ATPase protein transporter, SecA.[36] Walmsley et al. conducted an extensive study of the catalytic subunit of the *E. coli* arsenite transporter, ArsA, following the changes in intrinsic protein fluorescence along the MgATP catalytic cycle.[37] They concluded that ArsA exists in seven different conformational states along the reaction coordinate, with the rate-limiting step being a slow isomerization occurring after product release to a conformation productive to the binding of MgATP. We have shown that for all three complexes of Rad50 (Rad50, MR, and MR-D), chemistry or a preceding step is rate-limiting. Although the literature is limited, there does not appear to be one unifying theme for a rate-limiting step for ABC ATPases.

Search for a Catalytic Base. A catalytic base has long been implicated in phosphotransferases.[38−40] In ATPases, a catalytic base would abstract a proton from the attacking water, creating the hydroxyl anion ripe for nucleophilic attack of the γ-phosphate phosphorus. Currently, there are several hypotheses relating to the identity of the catalytic base in Rad50.[16,41,42] The two main candidates include the Walker B glutamate and the H-loop histidine. A competing hypothesis that has been proposed is "substrate-assisted catalysis", in which the γ-phosphate acts as the catalytic base.[43] This hypothesis appears to be unlikely on the basis of experimental and theoretical grounds.[44,45] A final hypothesis is that the transition state is highly asymmetric resembling a dissociative mechanism in which cleavage of the $\beta-\gamma$ phosphoryl bond precedes the formation of a bond with the catalytic water, which would diminish the catalytic contribution from a proton abstracting residue.[46]

There are conflicting results with regard to whether the Walker B glutamate is acting as the catalytic base. In the *Bacillus* multidrug resistance ATP (BmrA) ABC protein, Orelles et al. mutated the conserved glutamate and showed the complete loss of ATPase activity and the loss of Hoechst transport ability.[40] The authors concluded that the Walker B glutamate was the catalytic base. Moody et al. also showed that the E171Q mutation in the soluble cassette of *Methanococcus jannaschii* ABC transporter (MJ0796) lost all ATPase activity.[41] Alternatively, Carrier et al. mutated the Walker B glutamate residues (E552Q and E1197Q) in the mouse Mdr3 P-glycoprotein and showed loss of ATPase activity in their normal ATPase assay (following release of P_i) but did show vanadate trapping of 8-azido[α-^{32}P]ATP and showed by TLC analysis that the trapped nucleotide was in the ADP form.[47] On this basis, they concluded the Walker B glutamate is not the catalytic base.

In crystal structures of Rad50, the Walker B glutamate is forming a hydrogen bond to a water molecule in the first coordination sphere of the Mg^{2+} (PDB entries 3QKT and 1F2U[15,16]). It is also in a position to interact with what is presumed to be the catalytic water (3.9 Å). In the crystal structure of the *Thermatoga maritima* Rad50 structure, the Walker B glutamate is in a better position to act as the catalytic base [forms a hydrogen bond to the presumed catalytic water (2.6 Å) and the H-loop histidine (3.15 Å) (PDB entry

dx.doi.org/10.1021/bi500558d | *Biochemistry* 2014, 53, 5647−5660

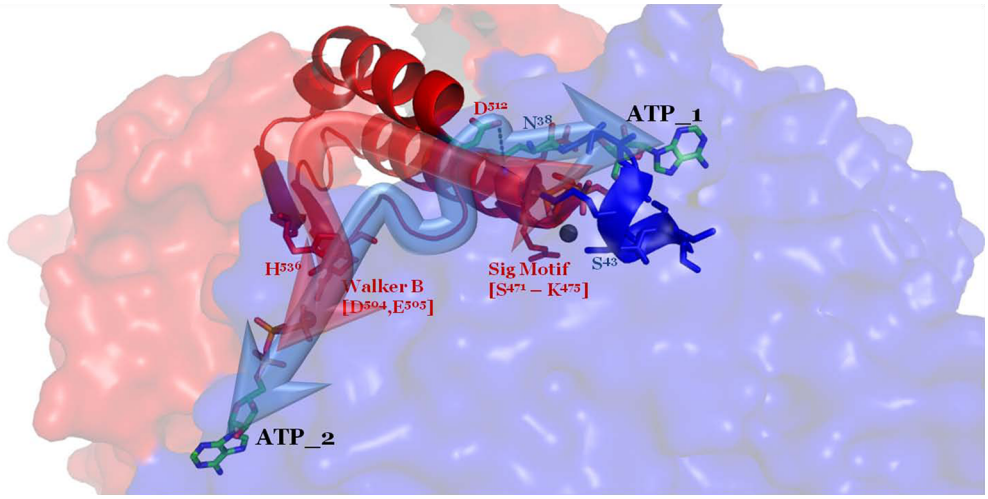

Figure 6. Proposed routes of cooperativity between Rad50 MgATP active sites. On the basis of the decrease in cooperativity of mutant proteins (Table 4), two routes of cooperativity are proposed. The first is an intramolecular (direct) route between the signature motif and the Walker B-motif (Red). The second proposed route is an intermolecular (indirect) route between the Walker B-motif of monomer A (red) and the Walker A-motif of monomer B (blue) mediated through the D-loop aspartate (D512) and the Walker A asparagine (N38). PDB entry 1F2U.

3QF7)].[14] Given these different positions, E505 may function as a catalytic residue, be involved in substrate binding, or both.

The affinity (K_d) and the Michaelis constant for MgATP of the E505Q mutant are essentially those of WT for Rad50 and the MR-D complex, respectively. Although E505Q is minimally catalytically deficient for Rad50 (~13-fold), the MR-D complex displays a diminution in activity closer to what one would expect for a catalytic base (320-fold). Considering interaction distances and the ability to abstract a proton, E505 and H536 remain the two best candidates for acting as a catalytic base.

Upon evaluation of the pH−rate profile for the WT MR-D complex, an ascending pK_a of 7.2 was determined. A similar pK_a was determined for the ubiquitous ABC transporter, HylB.[43] This could be indicative of the ionization state of an active site histidine (pK_a = 6.04[48]). When the pH−rate profile was determined for the H536Q mutant, the ascending pK_a was essentially unchanged (pK_a = 7.0), arguing against H536 acting as the catalytic base. Comparing the effect on catalysis between the alanine (145-fold) and glutamine (7-fold) mutants, we determined the most likely role for the H-loop histidine is in positioning the "catalytic" water for nucleophilic attack of either the γ-phosphate in an associative mechanism or metaphosphate in a dissociative mechanism. As stated in the Results, the other candidate for the catalytic base (E505) was unstable upon being mutated (E505Q) at pH <7.5 and could not be evaluated.

Another technique utilized to identify a catalytic base is following the rate in deuterium oxide [deuterium solvent isotope effect (DSIE)]. If the reaction involves a rate-limiting abstraction of a proton from water to create a more efficient nucleophile, the steady state rate should be considerably slower in D_2O. WT Rad50 and the WT MR-D complex steady state rates were essentially unchanged when they were measured in H_2O and D_2O. These data suggest that either abstraction of a proton from water is not rate-limiting or the reaction proceeds without the aid of a catalytic base. If the Walker B glutamate is the catalytic base, then mutation of this residue to a glutamine should result in chemistry becoming rate-limiting. The k_{H_2O}/k_{D_2O} ratio for this mutation was 1.14 ± 0.06 for Rad50 and 0.79 ± 0.02 for the MR-D complex. We interpret these results to suggest that the Walker B (E505Q) carboxylate is not acting as a catalytic base. Similar results were obtained by Zaitseva et al. for HylB (DSIE of 0.79).[43] The relative rates were also determined for the remaining mutations. The isotope effects for these mutations were slightly inverse, with the exception of that of the H536Q mutation that was closer to 1 (0.97) for Rad50 and slightly inverse for the MR-D complex (0.79).

Although the Walker B glutamate and the H-loop histidine mutations are catalytically deficient relative to the WT enzyme, the lack of a deuterium solvent isotope effect for the E505Q or H536A/Q mutations and the pH−rate profiles for WT and the H536A mutant argue against either residue acting as a catalytic base. This also argues against ATP hydrolysis proceeding through a tetrahedral associative transition state.[46]

Zaitseva et al. proposed that ATP hydrolysis proceeds by a substrate-assisted catalysis mechanism.[43] In this mechanism, the γ-phosphoryl acts as the catalytic base. If chemistry is rate-limiting, as we argue, a deuterium solvent isotope effect should be observed. Considering there is no change in the steady state rate, this mechanism is unlikely.

A dissociative mechanism for phosphoryl transfer is described by significant bond cleavage of the $\beta-\gamma$ bond prior to any significant bond formation of the incoming nucleophile.[49] In an associative mechanism, the γ-phosphoryl will experience an increase in negative charge characteristic. In a dissociative mechanism, the $\beta-\gamma$ bridging oxygen experiences the increase in negative charge characteristic. It has been proposed that the large decrease in activity resulting from the mutation of the Walker A lysine is due to the loss of stabilizing the large negative charge buildup in the transition state.[18,50] In the crystal structure of *Pfu* Rad50 (PDB entry 3QKT), the Walker A lysine is 2.76 Å from the nonbridging γ-phosphoryl oxygen and 3.75 Å from the $\beta-\gamma$ bridging nitrogen in AMPPNP. In the *T. maritima* structure (PDB entry 3QF7), the Walker A lysine is in a position that would support either mechanism (2.95 Å from the nonbridging γ-phosphoryl oxygen and 3.19 Å from the $\beta-\gamma$ bridging nitrogen of AMPPNP). Although these distances are more consistent with an associative transition state, it is possible the ATP analogue promotes a nonproductive conformation and the actual function for this lysine is to stabilize the increasing negative

dx.doi.org/10.1021/bi500558d | *Biochemistry* 2014, 53, 5647−5660

charge on the bridging oxygen during a dissociative transition state.

Cooperativity. It has long been postulated that the two NBDs of ABC ATPases are functionally coupled.[32,51−53] We have shown that the ATPase active sites of the MR-D complex are strongly cooperative (Hill coefficient of 2.4).[18] Several active site mutations decrease or abolish this cooperative nature (Table 2[17]). On the basis of these results, we propose two routes of cooperativity (Figure 6). The first route (red, Figure 6) relies on intramolecular contacts that connect the signature motif of one active site to the Walker B-motif of the other active site. This is essentially the route through the Rad50 "central cavity" that has been recently identified through a structural analysis of *Pfu* Rad50.[19] In the *Pfu* system, mutations of hydrophobic residues along the Rad50 signature helix broadly affect ATP-dependent functions.[19] The second route is intermolecular and connects the Walker B-motif of one active site through the D-loop aspartate to the Walker A asparagine. We also propose the complete loss of cooperativity observed for the Walker B residues is due to the mutations affecting both routes.

Interestingly, the degree of cooperativity does not appear to be linked to the allosteric activation by DNA. Although many mutations that displayed a loss of cooperativity also showed little to no activation (i.e., D504N and H536A), two mutations were activated to near WT levels. This is best displayed by the double mutant E505Q/H536A that has a Hill coefficient of 1.05 but is activated by DNA by ∼12-fold. When compared to the single mutants for the MR-D complex, the double mutant has no effect on k_{cat} (essentially the activity of H536A) and no effect on the Michaelis constant (essentially the same as E505Q) but has a synergistic effect in terms of DNA activation.

Nuclease Activity. To date, no mutation has significantly affected nuclease activity when ATP hydrolysis is not required (i.e., the 2-AP probe is in position 1 or 2). Although ATP-dependent nuclease activity (i.e., 2-AP probe in position 17) is always affected by a deficiency in ATP hydrolysis, there is not always a direct correlation between the two activities and appears to be more a function of which motif is perturbed (i.e., mutation) than the overall ATPase activity. Mutated residues in the Walker A-motif and D-loop region have less nuclease activity than mutations in the Walker B-motif or H-loop. For example, N38A (Walker A) exhibits a 103-fold decrease in k_{cat}, with a 50-fold decrease in nuclease activity; E505Q (Walker B) exhibits a 310-fold decrease in ATPase activity, but only a 3-fold decrease in nuclease activity.

CONCLUSION

We have mutated and functionally assigned residues in the Walker A-motif, Walker B-motif, and H-loop motifs. We have identified chemistry or a preceding conformational change as being rate-limiting for Rad50, Rad50 in the presence of Mre11, and the MR-D complex. The presence of a catalytic base has been discounted as a reaction mechanism because of the lack of a deuterium solvent isotope effect of the WT or mutant enzymes. On the basis of the steady state kinetics of active site mutants, two routes of cooperativity between the ATP active sites are proposed.

ASSOCIATED CONTENT

Supporting Information

Oligonucleotide sequences used in this study (Table S1) and Dynafit script for fitting stopped-flow fluorescence data of ADP and P_i time courses (Figure S1). This material is available free of charge via the Internet at http://pubs.acs.org.

AUTHOR INFORMATION

Corresponding Author

*E-mail: swn@iastate.edu. Phone: (515) 294-3434. Fax: (515) 294-0453.

Funding

This work was financially supported by National Science Foundation Grant MCB:1121693, the Roy J. Carver Charitable Trust, and Iowa State University.

Notes

The authors declare no competing financial interest.

ACKNOWLEDGMENTS

Use of the stopped-flow instrument (SFM-4000/MOS-500 from Biologic Science Instruments) was made possible through a generous gift from the Roy J. Carver Charitable Trust (Muscatine, IA).

ABBREVIATIONS

DSB, double-strand break; HR, homologous recombination; NHEJ, nonhomologous end joining; MR-D, Mre11/Rad50/DNA; ssDNA, single-stranded DNA; T4, bacteriophage T4; dsDNA, double-stranded DNA; *Pfu*, *P. furiosus*; SMC, structural maintenance of chromosomes; NBD, nucleotide binding domain; WT, wild-type; kan, kanamycin; amp, ampicillin; CBD, chitin binding domain; 2-AP, 2-aminopurine; ABC, ATP binding cassette; PARP1, poly[ADP-ribose] polymerase 1; PBP, phosphate binding protein; DSIE, deuterium solvent isotope effect; 7-MG, 7-methylguanosine; PNPase, purine nucleoside phosphorylase; PDRM, phosphodeoxyribomutase; MDCC, 7-(diethylamino)-3-[*N*-(2-maleimidoethyl)carbamoyl] coumarin; $S_{0.5}$, ATP concentration at half-maximal velocity, as calculated from a fit of the ATP saturation data to the Hill equation.

REFERENCES

(1) Kinoshita, E., van der Linden, E., Sanchez, H., and Wyman, C. (2009) RAD50, an SMC family member with multiple roles in DNA break repair: How does ATP affect function? *Chromosome Res. 17*, 277−288.

(2) Vilenchik, M. M., and Knudson, A. G. (2003) Endogenous DNA double-strand breaks: Production, fidelity of repair, and induction of cancer. *Proc. Natl. Acad. Sci. U.S.A. 100*, 12871−12876.

(3) Lahdesmaki, A., Taylor, A. M., Chrzanowska, K. H., and Pan-Hammarstrom, Q. (2004) Delineation of the role of the Mre11 complex in class switch recombination. *J. Biol. Chem. 279*, 16479−16487.

(4) Reina-San-Martin, B., Nussenzweig, M. C., Nussenzweig, A., and Difilippantonio, S. (2005) Genomic instability, endoreduplication, and diminished Ig class-switch recombination in B cells lacking Nbs1. *Proc. Natl. Acad. Sci. U.S.A. 102*, 1590−1595.

(5) Borde, V. (2007) The multiple roles of the Mre11 complex for meiotic recombination. *Chromosome Res. 15*, 551−563.

(6) Kuzminov, A. (1995) Collapse and repair of replication forks in *Escherichia coli*. *Mol. Microbiol. 16*, 373−384.

(7) Kogoma, T. (1997) Stable DNA replication: Interplay between DNA replication, homologous recombination, and transcription. *Microbiol. Mol. Biol. Rev. 61*, 212−238.

(8) Marrero, V. A., and Symington, L. S. (2010) Extensive DNA end processing by exo1 and sgs1 inhibits break-induced replication. *PLoS Genet. 6*, e1001007.

(9) Almond, J. R., Stohr, B. A., Panigrahi, A. K., Albrecht, D. W., Nelson, S. W., and Kreuzer, K. N. (2013) Coordination and processing of DNA ends during double-strand break repair: The role of the bacteriophage T4Mre11/Rad50 (MR) complex. *Genetics 195*, 739−755.
(10) Jones, P. M., O'Mara, M. L., and George, A. M. (2009) ABC transporters: A riddle wrapped in a mystery inside an enigma. *Trends Biochem. Sci. 34*, 520−531.
(11) Davidson, A. L., Dassa, E., Orelle, C., and Chen, J. (2008) Structure, function, and evolution of bacterial ATP-binding cassette systems. *Microbiol. Mol. Biol. Rev. 72*, 317−364.
(12) Walker, J. E., Saraste, M., Runswick, M. J., and Gay, N. J. (1982) Distantly related sequences in the α- and β-subunits of ATP synthase, myosin, kinases and other ATP-requiring enzymes and a common nucleotide binding fold. *EMBO J. 1*, 945−951.
(13) Moncalian, G., Lengsfeld, B., Bhaskara, V., Hopfner, K. P., Karcher, A., Alden, E., Tainer, J. A., and Paull, T. T. (2004) The rad50 signature motif: Essential to ATP binding and biological function. *J. Mol. Biol. 335*, 937−951.
(14) Lammens, K., Bemeleit, D. J., Mockel, C., Clausing, E., Schele, A., Hartung, S., Schiller, C. B., Lucas, M., Angermuller, C., Soding, J., Strasser, K., and Hopfner, K. P. (2011) The Mre11:Rad50 structure shows an ATP-dependent molecular clamp in DNA double-strand break repair. *Cell 145*, 54−66.
(15) Williams, G. J., Williams, R. S., Williams, J. S., Moncalian, G., Arvai, A. S., Limbo, O., Guenther, G., SilDas, S., Hammel, M., Russell, P., and Tainer, J. A. (2011) ABC ATPase signature helices in Rad50 link nucleotide state to Mre11 interface for DNA repair. *Nat. Struct. Mol. Biol. 18*, 423−431.
(16) Hopfner, K. P., Karcher, A., Shin, D. S., Craig, L., Arthur, L. M., Carney, J. P., and Tainer, J. A. (2000) Structural biology of Rad50 ATPase: ATP-driven conformational control in DNA double-strand break repair and the ABC-ATPase superfamily. *Cell 101*, 789−800.
(17) Herdendorf, T. J., and Nelson, S. W. (2011) Functional evaluation of bacteriophage T4 Rad50 signature motif residues. *Biochemistry 50*, 6030−6040.
(18) Herdendorf, T. J., Albrecht, D. W., Benkovic, S. J., and Nelson, S. W. (2011) Biochemical characterization of bacteriophage T4Mre11-Rad50 complex. *J. Biol. Chem. 286*, 2382−2392.
(19) Deshpande, R. A., Williams, G. J., Limbo, O., Williams, R. S., Kuhnlein, J., Lee, J. H., Classen, S., Guenther, G., Russell, P., Tainer, J. A., and Paull, T. T. (2014) ATP-driven Rad50 conformations regulate DNA tethering, end resection, and ATM checkpoint signaling. *EMBO J. 33*, 482−500.
(20) Kuzmic, P. (1996) Program DYNAFIT for the analysis of enzyme kinetic data: Application to HIV proteinase. *Anal. Biochem. 237*, 260−273.
(21) Krezel, A., and Bal, W. (2004) A formula for correlating pK_a values determined in D_2O and H_2O. *J. Inorg. Biochem. 98*, 161−166.
(22) Simopoulos, T. T., and Jencks, W. P. (1994) Alkaline phosphatase is an almost perfect enzyme. *Biochemistry 33*, 10375−10380.
(23) Bloom, L. B., Otto, M. R., Eritja, R., Reha-Krantz, L. J., Goodman, M. F., and Beechem, J. M. (1994) Pre-steady-state kinetic analysis of sequence-dependent nucleotide excision by the 3′-exonuclease activity of bacteriophage T4 DNA polymerase. *Biochemistry 33*, 7576−7586.
(24) De la Rosa, M. B., and Nelson, S. W. (2011) An interaction between the Walker A and D-loop motifs is critical to ATP hydrolysis and cooperativity in bacteriophage T4 Rad50. *J. Biol. Chem. 286*, 26258−26266.
(25) Blacklow, S. C., Raines, R. T., Lim, W. A., Zamore, P. D., and Knowles, J. R. (1988) Triosephosphate isomerase catalysis is diffusion controlled. Appendix: Analysis of triose phosphate equilibria in aqueous solution by ^{31}P NMR. *Biochemistry 27*, 1158−1167.
(26) Cole, P. A., Burn, P., Takacs, B., and Walsh, C. T. (1994) Evaluation of the catalytic mechanism of recombinant human Csk (C-terminal Src kinase) using nucleotide analogs and viscosity effects. *J. Biol. Chem. 269*, 30880−30887.
(27) Hopfner, K. P., Karcher, A., Shin, D., Fairley, C., Tainer, J. A., and Carney, J. P. (2000) Mre11 and Rad50 from *Pyrococcus furiosus*: Cloning and biochemical characterization reveal an evolutionarily conserved multiprotein machine. *J. Bacteriol. 182*, 6036−6041.
(28) Symington, L. S. (2002) Role of RAD52 epistasis group genes in homologous recombination and double-strand break repair. *Microbiol. Mol. Biol. Rev. 66*, 630−670.
(29) Falcon-Perez, J. M., Martinez-Burgos, M., Molano, J., Mazon, M. J., and Eraso, P. (2001) Domain interactions in the yeast ATP binding cassette transporter Ycf1p: Intragenic suppressor analysis of mutations in the nucleotide binding domains. *J. Bacteriol. 183*, 4761−4770.
(30) Cotten, J. F., and Welsh, M. J. (1998) Covalent modification of the nucleotide binding domains of cystic fibrosis transmembrane conductance regulator. *J. Biol. Chem. 273*, 31873−31879.
(31) Ramakrishnan, C., Dani, V. S., and Ramasarma, T. (2002) A conformational analysis of Walker motif A [GXXXXGKT (S)] in nucleotide-binding and other proteins. *Protein Eng. 15*, 783−798.
(32) Yang, R., Scavetta, R., and Chang, X. B. (2008) Interaction between the bound Mg·ATP and the Walker A serine residue in NBD2 of multidrug resistance-associated protein MRP1 plays a crucial role for the ATP-dependent leukotriene C4 transport. *Biochemistry 47*, 8456−8464.
(33) Mesecar, A. D., Stoddard, B. L., and Koshland, D. E. (1997) Orbital Steering in the Catalytic Power of Enzymes: Small Structural Changes with Large Catalytic Consequences. *Science 277*, 202−206.
(34) Hanson, P. I., and Whiteheart, S. W. (2005) AAA+ proteins: Have engine, will work. *Nat. Rev. Mol. Cell Biol. 6*, 519−529.
(35) Bjornson, K. P., Allen, D. J., and Modrich, P. (2000) Modulation of MutS ATP hydrolysis by DNA cofactors. *Biochemistry 39*, 3176−3183.
(36) Zito, C. R., Antony, E., Hunt, J. F., Oliver, D. B., and Hingorani, M. M. (2005) Role of a conserved glutamate residue in the *Escherichia coli* SecA ATPase mechanism. *J. Biol. Chem. 280*, 14611−14619.
(37) Walmsley, A. R., Zhou, T., Borges-Walmsley, M. I., and Rosen, B. P. (1999) The ATPase mechanism of ArsA, the catalytic subunit of the arsenite pump. *J. Biol. Chem. 274*, 16153−16161.
(38) Cole, P. A., Grace, M. R., Phillips, R. S., Burn, P., and Walsh, C. T. (1995) The role of the catalytic base in the protein tyrosine kinase Csk. *J. Biol. Chem. 270*, 22105−22108.
(39) Krepkiy, D., and Miziorko, H. M. (2004) Identification of active site residues in mevalonate diphosphate decarboxylase: Implications for a family of phosphotransferases. *Protein Sci. 13*, 1875−1881.
(40) Orelle, C., Dalmas, O., Gros, P., Di Pietro, A., and Jault, J. M. (2003) The conserved glutamate residue adjacent to the Walker-B motif is the catalytic base for ATP hydrolysis in the ATP-binding cassette transporter BmrA. *J. Biol. Chem. 278*, 47002−47008.
(41) Moody, J. E., Millen, L., Binns, D., Hunt, J. F., and Thomas, P. J. (2002) Cooperative, ATP-dependent association of the nucleotide binding cassettes during the catalytic cycle of ATP-binding cassette transporters. *J. Biol. Chem. 277*, 21111−21114.
(42) Tombline, G., Bartholomew, L. A., Urbatsch, I. L., and Senior, A. E. (2004) Combined mutation of catalytic glutamate residues in the two nucleotide binding domains of P-glycoprotein generates a conformation that binds ATP and ADP tightly. *J. Biol. Chem. 279*, 31212−31220.
(43) Zaitseva, J., Jenewein, S., Jumpertz, T., Holland, I. B., and Schmitt, L. (2005) H662 is the linchpin of ATP hydrolysis in the nucleotide-binding domain of the ABC transporter HlyB. *EMBO J. 24*, 1901−1910.
(44) Admiraal, S. J., and Herschlag, D. (2000) The Substrate-Assisted General Base Catalysis Model for Phophate Monoester Hydrolysis: Evaluation Using Reactivity Comparisons. *J. Am. Chem. Soc. 122*, 2145−2148.
(45) Hu, C.-H., and Brinck, T. (1999) Theoretical Studies of the Hydrolysis of the Methyl Phosphate Anion. *J. Phys. Chem. A 103*, 5379−5386.
(46) Hollfelder, F., and Herschlag, D. (1995) The nature of the transition state for enzyme-catalyzed phosphoryl transfer. Hydrolysis

of O-aryl phosphorothioates by alkaline phosphatase. *Biochemistry 34*, 12255−12264.
(47) Carrier, I., Julien, M., and Gros, P. (2003) Analysis of catalytic carboxylate mutants E552Q and E1197Q suggests asymmetric ATP hydrolysis by the two nucleotide-binding domains of P-glycoprotein. *Biochemistry 42*, 12875−12885.
(48) Wood, E. J. (1987) in *Data for biochemical research* (Dawson, R. M. C., Elliott, D. C., Elliott, W. H., and Jones, K. M., Eds.) 3rd ed., pp 580, Oxford Science Publications, Oxford, U.K.
(49) Maegley, K. A., Admiraal, S. J., and Herschlag, D. (1996) Ras-catalyzed hydrolysis of GTP: A new perspective from model studies. *Proc. Natl. Acad. Sci. U.S.A. 93*, 8160−8166.
(50) Herdendorf, T. J., and Miziorko, H. M. (2006) Phosphomevalonate kinase: Functional investigation of the recombinant human enzyme. *Biochemistry 45*, 3235−3242.
(51) Hou, Y. X., Riordan, J. R., and Chang, X. B. (2003) ATP binding, not hydrolysis, at the first nucleotide-binding domain of multidrug resistance-associated protein MRP1 enhances ADP·V_i trapping at the second domain. *J. Biol. Chem. 278*, 3599−3605.
(52) Hou, Y. X., Cui, L., Riordan, J. R., and Chang, X. B. (2002) ATP binding to the first nucleotide-binding domain of multidrug resistance protein MRP1 increases binding and hydrolysis of ATP and trapping of ADP at the second domain. *J. Biol. Chem. 277*, 5110−5119.
(53) Senior, A. E., al-Shawi, M. K., and Urbatsch, I. L. (1995) The catalytic cycle of P-glycoprotein. *FEBS Lett. 377*, 285−289.